

Adaptive Variational Quantum Imaginary Time Evolution Approach for Quantum Chemistry Calculations

Niladri Gomes Anirban Mukherjee Feng Zhang Thomas Iadecola  Cai-Zhuang Wang Kai-Ming Ho Peter P. Orth  Yong-Xin Yao* 

N. Gomes, A. Mukherjee, F. Zhang

Ames Laboratory, Ames, Iowa 50011, USA

T. Iadecola, C.-Z. Wang, K.-M. Ho, P.P. Orth, Y.-X. Yao

Ames Laboratory, Ames, Iowa 50011, USA

Department of Physics and Astronomy, Iowa State University, Ames, Iowa 50011, USA

*ykent@iastate.edu

Keywords: *quantum computation, quantum algorithms, quantum chemistry*

An adaptive variational quantum imaginary time evolution (AVQITE) approach is introduced that yields efficient representations of ground states for interacting Hamiltonians on near-term quantum computers. It is based on McLachlan’s variational principle applied to imaginary time evolution of variational wave functions, and avoids difficult nonconvex high-dimensional optimization that plagues other variational approaches such as the variational quantum eigensolver. The variational parameters evolve according to equations of motions that minimize the difference to the exact imaginary time evolution, which is quantified by the McLachlan distance. Rather than working with a fixed variational ansatz, where the minimal McLachlan distance is constrained by the quality of the ansatz, the adaptive method iteratively expands the ansatz along the dynamical path to ensure the McLachlan distance remains below a chosen threshold. AVQITE is used to prepare ground states of H_4 , H_2O and BeH_2 molecules and yields compact variational ansätze and ground state energies beyond chemical accuracy. Finally, quantum Lanczos calculations can also be naturally performed alongside AVQITE without additional quantum resource costs.

1 Introduction

Quantum computers promise to solve a subset of classically NP-hard problems in polynomial time at a bounded error probability, with quantum simulation as an important example [1]. In the long term, given access to fault-tolerant quantum computers, adiabatic state preparation followed by quantum phase estimation may become the standard algorithm to determine the ground state energy of a quantum chemistry Hamiltonian [2, 3, 4]. The required circuit depth, however, is beyond capabilities of near-term noisy intermediate-scale quantum (NISQ) devices, making low-depth hybrid quantum-classical algorithm such as the variational quantum eigensolver (VQE) much more promising to achieve quantum advantage [5, 6, 3, 4]. VQE takes the expectation value of a Hamiltonian, which is measured on a quantum device, as a cost function with a set of variational parameters that are optimized using classical algorithms. Excited-state calculations using VQE have also been proposed by modifying the energy cost function or low energy subspace expansion through linear response [5, 7, 8, 9].

Meanwhile, quantum imaginary time evolution (QITE) has been developed as an alternative approach to prepare ground states on quantum computers. QITE inherits the advantage of classical imaginary time evolution algorithms, which allow correlations to build faster than would be allowed by the Lieb-Robinson bound that governs real time evolution [10]. In QITE, the difficult high-dimensional nonconvex optimization of the energy cost function that arises in VQE is replaced by evolving the variational parameters along the imaginary time axis. The development of the QITE method includes two directions: the unitarized QITE approach represents the imaginary time propagator by a unitary one via least-square fitting [11], while the variational QITE (VQITE) approach is based on variational quantum simulation with fixed ansätze [12, 13]. The accuracy of the unitarized QITE method is tied to the size of correlation domains associated with the Hamiltonian. Specifically, the circuit depth grows exponentially with the domain sizes (being roughly the system’s correlation length) and linearly with the number of imaginary time steps. For practical implementations, strategies to reduce circuit complexity, e.g. by utilizing symmetries and effectively combining unitaries [14, 15, 16, 17], have been proposed. The VQITE

arXiv:2102.01544v2 [physics.chem-ph] 3 Feb 2021

method has the advantage of fixed circuit depth along the imaginary-time path, but its accuracy is limited by the fidelity of the variational ansatz in representing the ground state. While various strategies to construct variational ansätze have been reported during the development of VQE [18, 6, 19, 20, 21, 22], their accuracy can be system-dependent and the variational circuits can often be suboptimal [23, 24]. One promising strategy is to perform VQE with an adaptively generated ansatz, where operators are drawn from a predefined operator pool and iteratively added to the ansatz during the calculation. It was shown that adaptive VQE can yield highly accurate and compact variational ansätze for specific problems [25, 26, 27, 28, 29].

In this work, we develop an adaptive VQITE (AVQITE) method for variational quantum imaginary time evolution to efficiently prepare ground states of interacting fermion systems with high accuracy. The method generalizes the recently proposed adaptive variational quantum dynamics simulation (AVQDS) method [30] from real to imaginary time. Like AVQDS, the variational ansatz in AVQITE is automatically generated by choosing optimal multi-qubit Pauli rotation gates along the dynamical path to keep a measure of ansatz quality, the McLachlan distance, within a desired accuracy. We demonstrate the capabilities of AVQITE calculations by preparing the ground states of an H_4 chain and H_2O and BeH_2 molecules at representative bond lengths with increasing electron correlation effects. We find total energies to chemical accuracy with compact ansätze similar to qubit-ADAPT-VQE results, yet without resorting to the complex optimization of parameters in a high-dimensional nonconvex energy landscape. Furthermore, Quantum Lanczos calculations can be carried out together with AVQITE, leading to faster convergence to the ground state. We envision AVQITE, with its compact variational circuits and avoidance of explicit high-dimensional optimization, as a viable way to efficiently prepare ground states of interacting fermion systems (e.g., molecules) on NISQ devices.

2 AVQITE Algorithm

The AVQITE algorithm generalizes the recently introduced AVQDS approach [30] from real to imaginary time evolution. By time evolving a quantum state in imaginary time, it yields the ground state of a system as the final state. While the derivation of AVQITE resembles that of AVQDS, there are a few key differences that we point out in the following.

2.1 Variational Quantum Imaginary Time Evolution method

2.1.1 Algorithm

The theory of VQITE has been developed in reference [12] and has been used to find ground-state energies of H_2 and LiH molecules on classical simulators [12, 13]. Here, we review the VQITE formalism within the density matrix approach, which is insensitive to the global phase of the quantum state. Consider a system with Hamiltonian $\hat{\mathcal{H}}$ in a pure state $|\Psi\rangle$. The evolution of the density matrix $\hat{\rho} \equiv |\Psi\rangle\langle\Psi|$ under the imaginary-time propagator $e^{-\tau\hat{\mathcal{H}}}$ is governed by the Liouville–von Neumann-type equation [12, 31]

$$\frac{d\hat{\rho}}{d\tau} = \mathcal{L}[\hat{\rho}], \quad (1)$$

where the superoperator $\mathcal{L}[\hat{\rho}] = -\{\hat{\mathcal{H}}, \hat{\rho}\} + 2\langle\hat{\mathcal{H}}\rangle\hat{\rho}$ with the anticommutator $\{\hat{\mathcal{H}}, \hat{\rho}\} = \hat{\mathcal{H}}\hat{\rho} + \hat{\rho}\hat{\mathcal{H}}$, and the Hamiltonian expectation value $\langle\hat{\mathcal{H}}\rangle = \text{Tr}[\hat{\rho}\hat{\mathcal{H}}]$. The so-called imaginary time $\tau \in \mathbb{R}$ is a real positive parameter. For a generic variational ansatz $|\Psi[\boldsymbol{\theta}]\rangle$ with a real parameter vector $\boldsymbol{\theta}$ of dimension $N_{\boldsymbol{\theta}}$, the squared McLachlan distance L^2 is defined by the Frobenius norm of the difference between the varia-

tional and exact state propagations along the imaginary time axis, i.e. [12]:

$$\begin{aligned} L^2 &\equiv \left\| \sum_{\mu=1}^{N_{\theta}} \frac{\partial \hat{\rho}[\boldsymbol{\theta}]}{\partial \theta_{\mu}} \dot{\theta}_{\mu} - \mathcal{L}[\hat{\rho}] \right\|^2 \\ &= \sum_{\mu\nu} M_{\mu\nu} \dot{\theta}_{\mu} \dot{\theta}_{\nu} - 2 \sum_{\mu} V_{\mu} \dot{\theta}_{\mu} + \text{Tr}[\mathcal{L}[\hat{\rho}]^2], \end{aligned} \quad (2)$$

which is a quadratic function of the time derivatives $\{\dot{\theta}_{\mu} \equiv \partial \theta_{\mu} / \partial \tau\}$. The real symmetric $N_{\theta} \times N_{\theta}$ matrix M is specified as

$$M_{\mu\nu} = 2 \text{Re} \left[\frac{\partial \langle \Psi[\boldsymbol{\theta}] | \partial \Psi[\boldsymbol{\theta}] \rangle}{\partial \theta_{\mu}} \frac{\partial \langle \Psi[\boldsymbol{\theta}] | \partial \Psi[\boldsymbol{\theta}] \rangle}{\partial \theta_{\nu}} + \frac{\partial \langle \Psi[\boldsymbol{\theta}] | \partial \Psi[\boldsymbol{\theta}] \rangle}{\partial \theta_{\mu}} |\Psi[\boldsymbol{\theta}\rangle \frac{\partial \langle \Psi[\boldsymbol{\theta}] | \partial \Psi[\boldsymbol{\theta}] \rangle}{\partial \theta_{\nu}} |\Psi[\boldsymbol{\theta}\rangle \right]. \quad (3)$$

The real vector V of dimension N_{θ} is defined as

$$\begin{aligned} V_{\mu} &= 2 \text{Re} \left[-\frac{\partial \langle \Psi[\boldsymbol{\theta}] | \partial \Psi[\boldsymbol{\theta}] \rangle}{\partial \theta_{\mu}} \hat{\mathcal{H}} |\Psi[\boldsymbol{\theta}\rangle + \langle \Psi[\boldsymbol{\theta}] | \frac{\partial \langle \Psi[\boldsymbol{\theta}] | \partial \Psi[\boldsymbol{\theta}] \rangle}{\partial \theta_{\mu}} \langle \hat{\mathcal{H}} \rangle_{\boldsymbol{\theta}} \right] \\ &= 2 \text{Re} \left[-\frac{\partial \langle \Psi[\boldsymbol{\theta}] | \partial \Psi[\boldsymbol{\theta}] \rangle}{\partial \theta_{\mu}} \hat{\mathcal{H}} |\Psi[\boldsymbol{\theta}\rangle \right] \end{aligned} \quad (4)$$

with the abbreviation $\langle \hat{\mathcal{H}} \rangle_{\boldsymbol{\theta}} \equiv \langle \Psi[\boldsymbol{\theta}] | \hat{\mathcal{H}} | \Psi[\boldsymbol{\theta}\rangle$. The second term in the first line of equation (4) vanishes due to the normalization $\langle \Psi[\boldsymbol{\theta}] | \Psi[\boldsymbol{\theta}\rangle = 1$. The final term in Eq. (2) can be expressed in terms of the energy variance as

$$\text{Tr}[\mathcal{L}[\hat{\rho}]^2] = 2 \left(\langle \hat{\mathcal{H}}^2 \rangle_{\boldsymbol{\theta}} - \langle \hat{\mathcal{H}} \rangle_{\boldsymbol{\theta}}^2 \right) = 2 \text{var}_{\boldsymbol{\theta}}[\hat{\mathcal{H}}]. \quad (5)$$

The McLachlan variational principle amounts to minimizing the quadratic cost function L^2 with respect to $\{\dot{\theta}_{\mu}\}$. This leads to the following linear equations of motion:

$$\sum_{\nu} M_{\mu\nu} \dot{\theta}_{\nu} = V_{\mu}. \quad (6)$$

The second term in equation (3) originates from the global phase of the wavefunction [13, 12]. Below we adopt a purely real wave function ansatz in a pseudo-Trotter form (with odd number of Pauli-Y terms) for which the global phase contribution vanishes. Consequently, the density-matrix and wavefunction-based derivations reach exactly the same results.

The optimal McLachlan distance L^2 of the variational ansatz $\Psi[\boldsymbol{\theta}]$ given by

$$L^2 = 2 \text{var}_{\boldsymbol{\theta}}[\hat{\mathcal{H}}] - \sum_{\mu\nu} V_{\mu} M_{\mu\nu}^{-1} V_{\nu}. \quad (7)$$

VQITE is formulated in the exactly same form as real time variational quantum dynamics simulations (VQDS) [12, 30], with exception of the definition of vector V in Equation (4) due to the different super-operator $\mathcal{L}[\hat{\rho}]$ in the Liouville–von Neumann-type equation.

2.1.2 Flowchart

A typical VQITE calculation, which integrates the equation of motion (6) with a constant time step $\Delta\tau$ according to the Euler method, is illustrated in the green charts of Figure 1. Given a fixed variational ansatz initialized to a reference state $|\Psi_0\rangle$ that is easily prepared on a quantum computer, the energy expectation value is first measured. The convergence criterion, such as the energy difference between two consecutive steps, is checked. If the convergence condition is not satisfied, the real symmetric matrix M in Equation (3) and vector V in Equation (4) are determined, with which the step size $\Delta\boldsymbol{\theta}$ of the variational parameter vector $\boldsymbol{\theta}$ at time step $\Delta\tau$ is calculated. The ansatz state $|\Psi[\boldsymbol{\theta}]\rangle$ with the updated parameters triggers another iteration until convergence is reached. Note that the energy variance $\text{var}_{\boldsymbol{\theta}}[\hat{\mathcal{H}}]$ provides a quality measure of the variational ansatz in approximating the ground state.

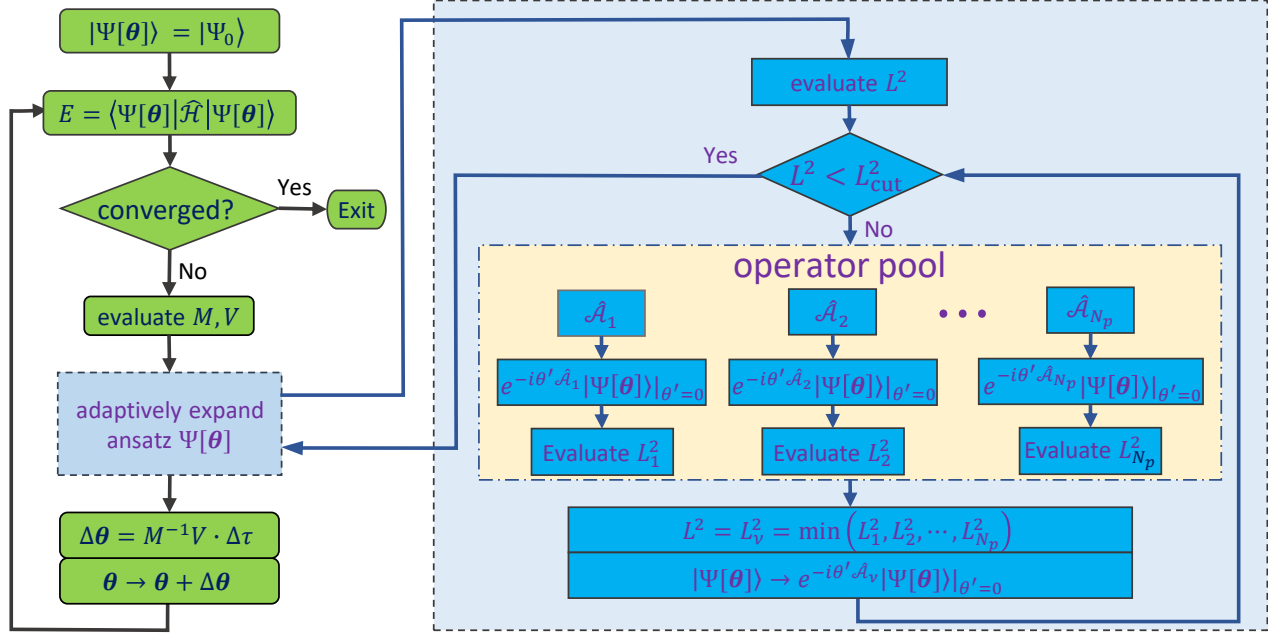


Figure 1: **Schematic illustration of variational quantum imaginary time evolution algorithm, with an additional module to adaptively expand the ansatz.** The green flowchart on the left shows a typical VQITE calculation. In AVQITE, a module (blue) is introduced to adaptively expand the variational ansatz by selectively appending parametric rotation gates to keep the McLachlan distance L^2 under a threshold L^2_{cut} along the imaginary-time evolution path.

2.2 Adaptive Variational Quantum Imaginary Time Evolution Method

2.2.1 Algorithm and Flowchart

The VQITE formalism is presented for a generic wave function ansatz. In the development of VQE, variational ansätze $|\Psi[\theta]\rangle = \hat{\mathcal{U}}[\theta] |\Psi_0\rangle$ with two different forms of the unitary operator $\hat{\mathcal{U}}[\theta]$ acting on a reference state $|\Psi_0\rangle$ have been proposed. In hardware efficient ansätze, the unitary operator $\hat{\mathcal{U}}[\theta]$ is a product of parametrized native gates of the real device, e.g., single-qubit rotation gates plus two-qubit entangling gates [18]. Alternatively, at a higher algorithmic level, $\hat{\mathcal{U}}[\theta]$ can be expressed as a product of N_θ multi-qubit rotation gates in a pseudo-Trotter form:

$$|\Psi[\theta]\rangle = \prod_{\mu=0}^{N_\theta-1} e^{-i\theta_\mu \hat{\mathcal{A}}_\mu} |\Psi_0\rangle, \quad (8)$$

where $\hat{\mathcal{A}}_\mu$ are Hermitian operators. The unitary coupled cluster ansatz and its variants [6, 19, 20], the Hamiltonian variational ansatz [21], and the ansatz in the quantum approximate optimization algorithm (QAOA) all belong to this category [22]. In AVQITE, we adopt a variational ansatz in the above form (8), and allow the number of $\hat{\mathcal{A}}$ -operators to be dynamically expanded along the imaginary-time evolution path to maintain high accuracy in representing the evolving quantum state, as shown in the blue module of Figure 1.

The initial steps of an AVQITE calculation are the same as those of a VQITE calculation, with the exception of great flexibility in the choice of initial ansatz $|\Psi[\theta]\rangle$. While the simulation accuracy is tied to the initial ansatz in VQITE calculations, an AVQITE calculation monitors the quality of $|\Psi[\theta]\rangle$ in representing the evolving quantum state and adaptively expands the form of $|\Psi[\theta]\rangle$ to maintain a fixed accuracy. In fact, AVQITE calculations can simply take any $|\Psi_0\rangle$ as the initial ansatz. For convenience, we use a product state as our initial state in all our calculations below, which is easily prepared on a quantum processor unit (QPU). In the first iteration where no variational parameters are present, the McLachlan distance L^2 in Equation (7) is determined by the energy variance $\text{var}[\hat{\mathcal{H}}]$ in state $|\Psi_0\rangle$, which

is generally larger than the threshold L_{cut}^2 , since $|\Psi_0\rangle$ is not an eigenstate of $\hat{\mathcal{H}}$. As a result, a predefined operator pool is scanned and an operator \hat{A}_ν is chosen to construct a unitary $e^{-i\theta'\hat{A}_\nu}$ to be appended to the variational ansatz $|\Psi[\boldsymbol{\theta}]\rangle$, which produces minimal McLachlan distance, as illustrated in Figure 1. The additional parameter θ' associated with the new operator is always initialized to zero to keep the imaginary time evolution of the variational state continuous. Nevertheless, the McLachlan distance can still be reduced by addition of $e^{-i\theta'\hat{A}_\nu}$, because it involves derivatives of the ansatz. The adaptive procedure of selectively appending a new unitary to the ansatz continues until the updated McLachlan distance satisfies $L^2 < L_{\text{cut}}^2$. The expanded variational parameter vector $\boldsymbol{\theta}$ is subsequently updated at the imaginary time step as in VQITE, and new iterations proceed until energy convergence is reached.

2.2.2 Important Technical Details

The accuracy of AVQITE calculations is controlled by the McLachlan distance threshold L_{cut}^2 , while the ability to reach a compact final ansatz $|\Psi[\boldsymbol{\theta}]\rangle$ is tied to the operator pool. For quantum chemistry calculations, different ways to efficiently construct operator pools and pool completeness conditions have been extensively discussed in the context of adaptive approaches to VQE [25, 26, 27]. The fermionic operator pool proposed in reference [25] is composed of the single excitation operators and double excitation operators with respect to a Hartree-Fock (HF) reference state. When translated to a qubit representation using encoding methods such as Jordan-Wigner (JW) mapping [32], a single excitation operator can result in a weighted sum of two Pauli strings, and six Pauli strings for a double excitation. Here a Pauli string is defined as a product of single qubit Pauli operators, namely X, Y and Z . Alternatively, a qubit operator pool can also be constructed directly with rudimentary Pauli strings [26, 27]. Compared with fermionic operator pools, adaptive-VQE calculations with qubit operator pools generate variational ansätze with considerably shallower circuits at the price of more variational parameters. As the complex nonconvex optimization problem in the high-dimensional parameter space of VQE is completely avoided in AVQITE, the qubit operator pool is therefore very appealing and adopted in the following AVQITE calculations. In the AVQITE calculations, we construct a qubit operator pool by choosing all the Pauli strings present in the fermionic single and double excitation operators of the unitary coupled cluster ansatz [6, 19]. The parity mapping is used to transform the fermionic excitation operators to qubit operators [33, 34], as fermion to qubit mappings other than JW have not been studied before in the context of operator pool construction [26]. Since the fermionic excitation operators are real, every Pauli string in the operator pool contains an odd number of Pauli Y operators and is therefore antisymmetric. The unitaries in equation (8) are thus real and an initially real wave function (i.e. with real coefficients) remains real when evolving along the imaginary time path. Consequently, the expression $\frac{\partial \langle \Psi[\boldsymbol{\theta}] |}{\partial \theta_\mu} |\Psi[\boldsymbol{\theta}]\rangle = \langle \Psi_{\mu-1} | i\hat{A}_\mu | \Psi_{\mu-1} \rangle$ in Eq. (3), where $|\Psi_\mu[\boldsymbol{\theta}]\rangle = \prod_{\mu'=0}^{\mu} e^{-i\theta_{\mu'}\hat{A}_{\mu'}} |\Psi_0\rangle$, vanishes for any μ . Therefore, the second term of M in Eq. (3) which originates from the global phase of the wavefunction vanishes, and the density-matrix and wavefunction-based approaches lead to exactly the same results. As discussed previously, the VQITE and real time VQDS calculations amount to integrate an equation of motion of the same form (6). While sufficiently small step size is necessary to maintain the high accuracy of VQDS results along the dynamical path, relatively bigger step size can be adopted in VQITE because only the final state is of interest [14]. In the following AVQITE calculations of molecules in Hartree atomic units, we find $\Delta\tau = 0.1$ works well, which leads to ground state solution of chemical accuracy with relatively fewer steps.

2.2.3 Implementation Strategies on Real Devices

The implementation of AVQITE amounts to measuring the symmetric matrix M in Eq. (3), the vector V in Eq. (4) and the scalars $\langle \hat{\mathcal{H}} \rangle_{\boldsymbol{\theta}}$, $\langle \hat{\mathcal{H}}^2 \rangle_{\boldsymbol{\theta}}$ on a quantum device, all of which has been discussed in the context of VQITE in reference [6, 35]. The energy $\langle \hat{\mathcal{H}} \rangle_{\boldsymbol{\theta}}$ can be obtained as a weighted sum of expectation values of the Pauli strings in the Hamiltonian, a procedure often termed ‘‘Hamiltonian averaging’’ [6]. The expectation value $\langle \hat{\mathcal{H}}^2 \rangle_{\boldsymbol{\theta}}$ can be obtained similarly by replacing $\hat{\mathcal{H}}$ with $\hat{\mathcal{H}}^2$. The circuit

implementation to measure V , which is essentially the energy gradient, has also been discussed in the context of VQE optimization [36, 37]. The proposed indirect measurement circuit introduces an ancillary qubit with a Hadamard-type test. Two controlled-unitary gates, specifically, controlled multi-qubit Pauli gates, need to be implemented. As the implementation of controlled-unitary gates can be challenging for NISQ devices, general strategies to replace indirect measurements by direct measurements have also been proposed [38]. It is especially appealing to use the parameter-shift rule to evaluate the energy gradient V [39, 40, 41, 42], as it only requires some additional measurements of Hamiltonian expectation values at shifted parameters, without necessity of introducing new circuits. For the matrix element $M_{\mu\nu} = 2 \operatorname{Re} \left[\frac{\partial \langle \Psi[\boldsymbol{\theta}] |}{\partial \theta_\mu} \frac{\partial \langle \Psi[\boldsymbol{\theta}] |}{\partial \theta_\nu} \right]$ in Eq. (3), where we have the vanishing global phase term with the pseudo-Trotter ansatz (8), the diagonal element can be simplified to $M_{\mu\mu} = 2 \langle \Psi_\mu[\boldsymbol{\theta}] | \hat{\mathcal{A}}_\mu^2 | \Psi_\mu[\boldsymbol{\theta}] \rangle$, where $|\Psi_\mu[\boldsymbol{\theta}]\rangle = \prod_{\mu'=0}^{\mu} e^{-i\theta_{\mu'} \hat{\mathcal{A}}_{\mu'}} |\Psi_0\rangle$. This can be measured with the Hamiltonian averaging method for the Hermitian operator $\hat{\mathcal{A}}_\mu^2$. Because $\hat{\mathcal{A}}_\mu$ is a single Pauli string for the qubit operator pools adopted here, $\hat{\mathcal{A}}_\mu^2$ is an identity operator and $M_{\mu\mu} = 2$. The off-diagonal elements of M can be simplified to $M_{\mu\nu} = 2 \operatorname{Re} \left[-\frac{\partial \langle \Psi_\nu[\boldsymbol{\theta}] |}{\partial \theta_\mu} i \hat{\mathcal{A}}_\nu | \Psi_\nu[\boldsymbol{\theta}] \rangle \right]$ with $\mu < \nu$, which bears the same form as V in Eq. (4) with $\hat{\mathcal{H}} \rightarrow i \hat{\mathcal{A}}_\nu$ and can also be measured using the parameter-shift rule [39].

2.2.4 Quantum Lanczos Calculation

The focus of the QITE approach lies on the final quantum state, which converges to the ground state for large enough time. Within QITE, all previous quantum states along the path are discarded. In contrast, the quantum Lanczos (QL) method was developed to achieve a more efficient calculations of ground and excited state energies by exploiting information contained in all quantum states along the path [11]. The essence of QL is to diagonalize the Hamiltonian within the Krylov subspace spanned by a subset of imaginary-time states $\{|\Psi_n\rangle = C_n e^{-n\Delta\tau\hat{\mathcal{H}}} |\Psi_0\rangle\}$ with even time step indices $n = 0, 2, \dots, N$ and normalization constants C_n . In the classical Lanczos algorithm, the reduced Hamiltonian in the Krylov subspace is brought to a tridiagonal form by sequentially applying the Hamiltonian on orthonormalized Krylov basis vectors [43]. While for convenience, QL directly represents the reduced Hamiltonian $\hat{\mathcal{H}}$ in the normalized basis $\{|\Psi_n\rangle\}$ characterized by an overlap matrix $S_{nn'} = \frac{C_n C_{n'}}{C_{(n+n')/2}^2}$. As the normalization coefficient $C_{(n+n')/2}$ is used, only the even- n imaginary-time states (for which $(n+n')/2$ is an integer) are chosen for the construction of the Krylov subspace. Accordingly, the dense Hamiltonian matrix elements can be evaluated as $H_{nn'} = S_{nn'} E_{(n+n')/2}$, where the expectation value $E_n \equiv H_{nn} = \langle \Psi_n | \hat{\mathcal{H}} | \Psi_n \rangle$. The normalization coefficient C_n can be calculated recursively as $C_n^{-2} = C_{n-1}^{-2} (1 - 2\Delta\tau E_{n-1} + \mathcal{O}(\Delta\tau^2))$ with $C_0 = 1$. Therefore, only the expectation values of the Hamiltonian $\{E_n\}$ are needed to set up the generalized eigenvalue equation in the Krylov subspace for QL. As $\{E_n\}$ are readily available in an AVQITE calculation, a QL calculation can be efficiently performed alongside AVQITE to get the energy eigenvalues with no additional quantum resource costs. Nevertheless, as the Lanczos eigenvector is expressed as a linear combination of imaginary time states, it can be much more involved to measure expectation values of other observables beyond energy on a quantum computer [44].

3 AVQITE calculations of molecules

The *ab initio* nonrelativistic molecular electron Hamiltonian is given by

$$\hat{\mathcal{H}} = \sum_{pq} \sum_{\sigma} h_{pq} \hat{c}_{p\sigma}^\dagger \hat{c}_{q\sigma} + \frac{1}{2} \sum_{pqrs} \sum_{\sigma\sigma'} h_{pqrs} \hat{c}_{p\sigma}^\dagger \hat{c}_{r\sigma'}^\dagger \hat{c}_{s\sigma'} \hat{c}_{q\sigma}, \quad (9)$$

where the one-electron core part $h_{pq} = \int d\mathbf{r} \phi_p^*(\mathbf{r}) (\mathcal{T} + \mathcal{V}_{ion}) \phi_q(\mathbf{r})$, and the two-electron Coulomb integral is obtained as

$$h_{pqrs} = \iint d\mathbf{r} d\mathbf{r}' \phi_p^*(\mathbf{r}) \phi_r^*(\mathbf{r}') \mathcal{V}_{ee}(|\mathbf{r} - \mathbf{r}'|) \phi_s(\mathbf{r}') \phi_q(\mathbf{r}). \quad (10)$$

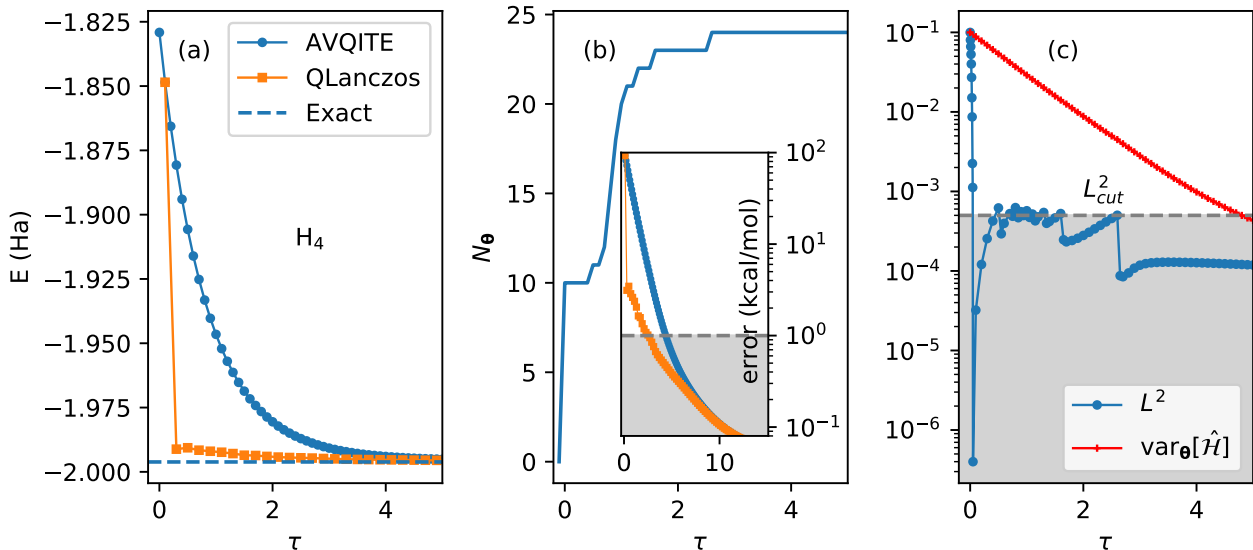


Figure 2: **AVQITE calculation for H_4 chain.** Along the imaginary time path of $\tau = N\Delta\tau$, the total energies of H_4 from AVQITE and quantum Lanczos calculations are shown in panel (a), the number of variational parameters N_θ in (b), and the McLachlan distance L^2 and energy variance $\text{var}_\theta[\hat{\mathcal{H}}]$ in (c). The exact full configuration interaction result is shown as the dashed line in (a) for reference. The total energy errors $E - E_{\text{Exact}}$ are plotted in the inset of (b), with the shaded area denoting chemical accuracy. The chosen threshold $L_{\text{cut}}^2 = 5 \times 10^{-4}$ is indicated by a dashed line in (c).

Here p, q, r, s are composite indices for atom and orbital, and σ is the spin index. \mathcal{T} , \mathcal{V}_{ion} and \mathcal{V}_{ee} are the kinetic energy, ionic potential operator and Coulomb interaction operator, respectively. The standard STO-3G minimal basis set is adopted for the basis orbital functions $\{\phi(\mathbf{r})\}$. In the following AVQITE calculations, the *PySCF* quantum chemistry package is first used to generate the molecular Hamiltonian (9) and produce the restricted Hartree-Fock(HF) solution [45]. A basis transformation from atomic orbitals to molecular orbitals is performed to the Hamiltonian (9) for the convenience of preparation of the initial HF state as a tensor product state on the quantum computer. The parity transformation is applied to get the qubit representation of the molecular Hamiltonian, where two qubits are tapered due to the Z_2 symmetry from total electron number and total spin conservation [33, 46, 47].

In figure 2 we illustrate a detailed numerical AVQITE calculation of an H_4 chain molecule at a uniform bond length $R = 1.5\text{\AA}$, where significant electron correlation effects are present. Starting with the initial Hartree-Fock state $|\Psi_0\rangle$, the total energy monotonically decreases and converges toward the exact result with increasing imaginary time $\tau = N\Delta\tau$ at $\Delta\tau = 0.1$, as shown by the blue circles in figure 2(a). The associated error, which is defined as the difference between the AVQITE energy and the exact result from a full configuration interaction (FCI) calculation $E - E_{\text{Exact}}$, is shown in the inset of figure 2(b) on a log scale. The AVQITE calculation reaches chemical accuracy of 1 kcal/mol after $\tau = 4.7$. The quantum state fidelity [1], which is defined as the squared overlap between the ansatz state and the exact ground state $|\langle\Psi[\theta]|\Psi_{\text{Exact}}\rangle|^2$, goes beyond 99.9%. The number of variational parameters N_θ , or equivalently the number of multi-qubit Pauli rotation gates, increases at several imaginary time steps and flattens at 24. For comparison, the qubit-ADAPT VQE calculation of H_4 using the same operator pool generates a final ansatz of 30 variational parameters upon reaching chemical accuracy. Specific information about the McLachlan distance L^2 is plotted in figure 2(c), where L^2 is reduced below the threshold $L_{\text{cut}}^2 = 5 \times 10^{-4}$ by adaptively expanding the variational ansatz whenever the initial value $L^2 > L_{\text{cut}}^2$ at any time step. Together with L^2 , the energy variance $\text{var}_\theta[\hat{\mathcal{H}}]$ along the imaginary path is shown to be almost linear on a semi-log scale, implying an exponential convergence. In fact, the AVQITE total energies $E(\tau)$ can also be fitted with an exponential function, $E(\tau) = E_\infty + e^{-a\tau}$, with $E_\infty = -1.9957$ Ha in the infinite time step limit, which is within chemical accuracy with an error of 0.2 kcal/mol. Alternatively, one can fit a function $E(\text{var}_\theta[\hat{\mathcal{H}}]) = E_0 + b\text{var}_\theta[\hat{\mathcal{H}}]$ due to the approximately linear relation between E and $\text{var}_\theta[\hat{\mathcal{H}}]$ in the numerical results, where $E_0 = -1.9959$ Ha in the zero-variance limit is also very accurate with an

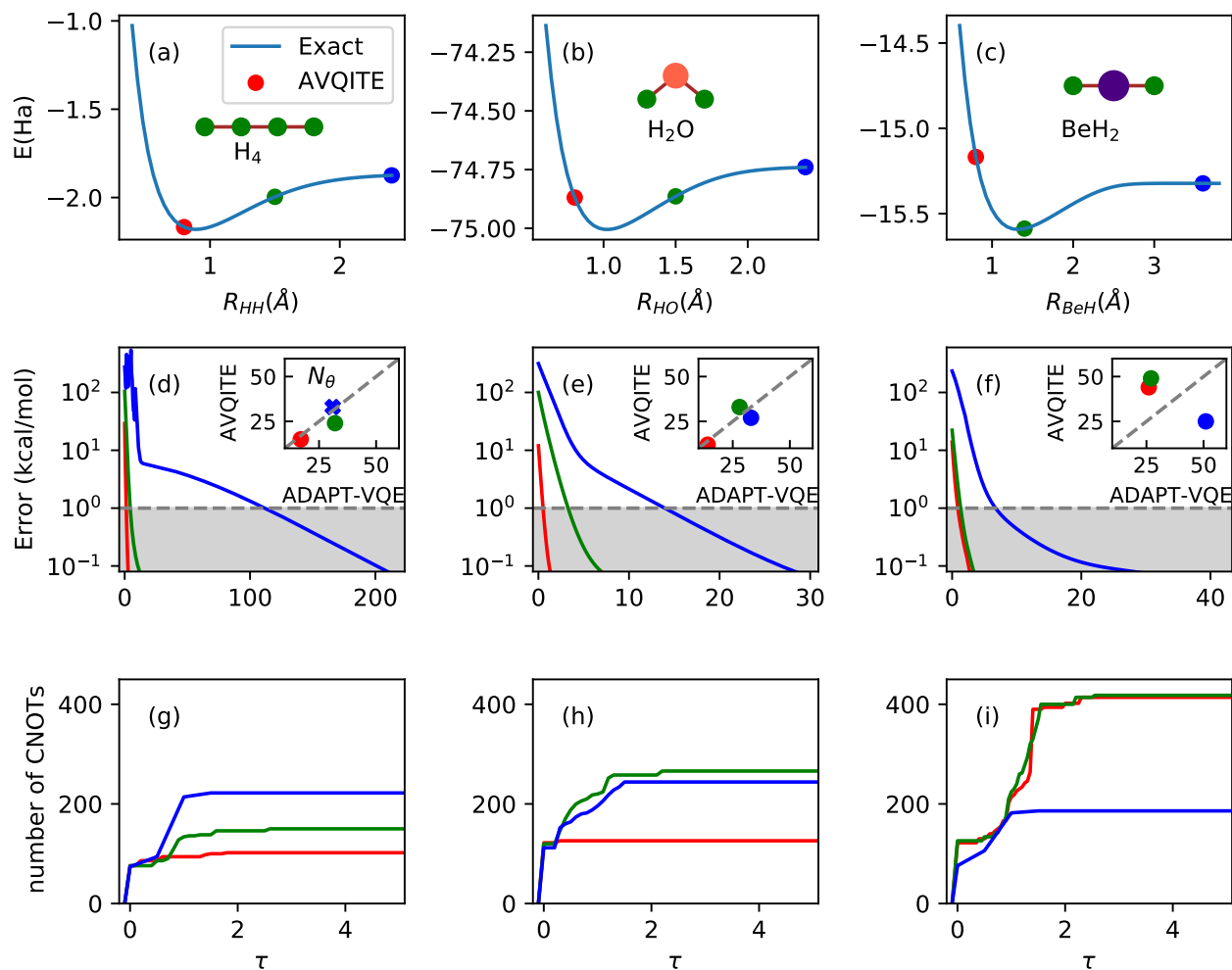


Figure 3: **AVQITE calculations of molecules with varying electron correlations.** Upper panels: AVQITE total energies of H_4 , H_2O and BeH_2 molecules at three bond lengths colored by red, green and blue. The exact potential energy curves from FCI calculations are also shown for reference. Middle panels: AVQITE energy error, $E - E_{Exact}$, as a function of imaginary time step $\tau = N\Delta\tau$ for the molecules at bond lengths with the same color coding. The shaded area indicates errors smaller than chemical accuracy. Insets: Number of variational parameters N_θ of the AVQITE ansatz vs. that for qubit-ADAPT-VQE when the energy accuracy reaches 0.1 mHa. The symbol “ \times ” indicates qubit-ADAPT-VQE does not converge. Lower panels: Dependence of the number of CNOT gates in the AVQITE state preparation circuit as a function of imaginary time for each set of molecules.

error 0.1 kcal/mol.

The quantum Lanczos results, which are conveniently calculated along with AVQITE at no additional quantum resource cost, are plotted as orange squares in figure 2(a) for the total energy, with the error shown in the inset of panel (b). The QL calculation converges relatively faster than AVQITE, since the reduced Lanczos Hamiltonian encodes information beyond the latest quantum state. Because the QL method is generally susceptible to numerical inaccuracies and the way to evaluate the Hamiltonian and overlap matrix in the Krylov subspace used in the QL method accumulates sizable errors, excited states cannot be directly accessed in the current QL calculations.

To demonstrate the general applicability of the AVQITE approach in generating compact ground state ansätze, we perform AVQITE calculations for H_4 chains at bond length $R_{HH} = 0.8\text{\AA}$, 1.5\AA , 2.4\AA , H_2O at $R_{OH} = 0.8\text{\AA}$, 1.5\AA , 2.4\AA , and BeH_2 at $R_{BeH} = 0.8\text{\AA}$, 1.4\AA , and 3.6\AA , as shown in figure 3. This benchmark set covers a variety of directional covalent bonding and electron correlation effects, with atomic states of spin singlet, doublet and triplet in the dissociation limit. In figure 3(a) we show the AVQITE energies of H_4 at three bond lengths colored in red, green and blue, which agree with the FCI results beyond chemical accuracy. The detailed error convergence, $E - E_{Exact}$, as a function of imaginary time step

$\tau = N\Delta\tau$ is shown in panel (d). With increasing bond length or correlation energy, the critical imaginary time τ_c , which is defined as the time where chemical accuracy is reached, generally increases. Here the correlation energy is defined as the difference between the HF and FCI energies, which corresponds to the initial AVQITE energy error as the AVQITE ansatz starts with the HF state. At $R_{\text{HH}} = 2.4\text{\AA}$ proximate to the atomic limit, the critical time step increases significantly to $\tau_c \approx 110$. However, as observed earlier in numerical step-merged QITE calculations [14], one can choose a bigger step size $\Delta\tau$ for molecules at larger bond length to reduce the number of imaginary time steps N . In this case, $\Delta\tau$ is increased from 0.1 to 0.5 to speed up the convergence, although sizable energy fluctuations are present in the initial time steps. The number of controlled-NOT gates (CNOTs) generally increases in the initial steps and levels off for τ above 3, as shown in panel (g). The maximal number of CNOTs reaches 250 for H_4 at $R_{\text{HH}} = 2.4\text{\AA}$. Here the number of CNOTs is estimated by the rule that each multi-qubit rotation gate $e^{-i\theta\hat{\sigma}}$ with Pauli string $\hat{\sigma}$ of length p needs $2(p-1)$ CNOTs (assuming all-to-all connectivity) [1]. Moving on to the AVQITE calculations of H_2O and BeH_2 at representative bond lengths, the error convergence behavior generally remains similar to the H_4 calculations, with final energies beyond chemical accuracy. Likewise, the number of CNOTs in the AVQITE state preparation circuit generally increases initially and levels off for $\tau > 3$. The total number of CNOTs remains close to or under 400. Remarkably, the positive correlation between the number of CNOTs in the AVQITE ansatz and correlation energy, which seems to exist in the calculations of H_4 , does not apply to H_2O and BeH_2 . The AVQITE state preparation circuits in the test-set are generally over one order of magnitude shallower than the original UCCSD ansatz. In the insets of the middle panels, we show that the number of variational parameters N_θ of the AVQITE ansatz is generally quite close to that of the qubit-ADAPT-VQE approach at the energy accuracy of 0.1 mHa, albeit with appreciable difference in the case of BeH_2 . The H_4 chain at $R_{\text{HH}} = 2.4\text{\AA}$ marked by a blue cross symbol in the inset of Fig. 3(d) represents an interesting example, where the qubit-ADAPT-VQE becomes trapped in a local minimum with energy 15 mHa higher than the ground-state energy. The qubit-ADAPT-VQE method is implemented according to references [23, 26], where the variational ansatz in a new generation with an additional parameterized unitary is optimized using the conjugate-gradient method at the optimal solution of the previous generation. This implies that the energy cost function is optimized along a continuous parameter path, which could lead to a local minimum with vanishing gradients in a generally nonconvex high-dimensional energy landscape, as exemplified here. This is related with the general barren plateau problem where the optimization of random circuits is trapped in a flat cost function region in the parameter space [48]. Various techniques to address the barren plateau problem have been proposed, including the block-identity initialization strategy [49], and entanglement devised mitigation techniques [50]. In fact, a modified qubit-ADAPT-VQE calculation, which successively adds unitaries in accordance with the AVQITE calculation and optimizes the ansatz initialized at the AVQITE parameter values already reaches the accuracy of 0.1mHa with the first 31 unitaries out the total 33 unitaries in the AVQITE ansatz. This implies a proper combination of qubit-ADAPT-VQE and AVQITE can be mutually beneficial.

Going forward to larger systems, the number of terms in the *ab initio* Hamiltonian in Eq. (9) scales as N_{orb}^4 for molecules with N_{orb} basis orbitals due to the presence of two-body Coulomb interactions. The resource cost for straightforward evaluation of $\langle \hat{\mathcal{H}}^2 \rangle_\theta$ then scales as N_{orb}^8 . The operator pool size grows as N_{orb}^4 if the Pauli operators are obtained from the single and double excitations of the UCCSD ansatz. Therefore, the resource cost for an AVQITE calculation, limited by measuring V in Eq. (4) and $\langle \hat{\mathcal{H}}^2 \rangle_\theta$, scales as N_{orb}^8 , because all the measurements can be achieved using the Hamiltonian averaging method with the help of the parameter-shift rule as discussed previously in Sec. 2.2.3. Multiple techniques from the literature can be utilized to reduce this high-order polynomial scaling. The low-rank tensor factorization of the Hamiltonian coefficients h_{pq} and h_{pqrs} reduces the number of distinct measurement circuits for $\langle \hat{\mathcal{H}} \rangle_\theta$ from N_{orb}^4 to linear scaling, with small overhead of basis transformation through Givens rotation [51, 52, 53]. Likewise, the resource cost for measuring $\langle \hat{\mathcal{H}} \rangle_\theta^2$ can be reduced to quadratic scaling. Scaling reduction based on reduced density matrices is another interesting approach [54]. Various approaches to generate efficient operator pools, including minimal pools whose size scale linearly with the qubit-basis dimension, have been discussed [23, 26, 27]. Finally, AVQITE can be applied to reduced

“low energy” models in quantum chemistry such as those that arise within the complete active space self-consistent field method (CASSCF) [55]. More generally, it can be used as impurity solver for quantum embedding approaches like the rotationally invariant Gutzwiller embedding and density-matrix embedding methods [56, 57, 58, 59, 60, 61, 62], extending its application to larger molecules and solid state materials.

4 Conclusion

The adaptive variational quantum imaginary time evolution (AVQITE) approach is developed by generalizing the recently proposed adaptive quantum dynamics simulation (AVQDS) method from real time to imaginary time. We present benchmark quantum chemistry calculations on H_4 , H_2O and BeH_2 with different chemical bonding character and atomic spin multiplicity upon dissociation limit. They demonstrate the general applicability of AVQITE to finding accurate and compact variational ansätze for interacting many-electron models. The key advantage of AVQITE over adaptive VQE approaches is that it bypasses the complicated nonconvex optimization problem in high-dimensional parameter space by performing energy cost function minimization along a single imaginary time axis. With the favorable polynomial scaling of the AVQITE calculations which automatically generates compact variational ansätze of high accuracy, we envision feasible follow-up applications of this method on NISQ devices to calculate molecular ground-state properties, with excited states also accessible if combined with techniques like the folded spectrum method [5, 6, 63, 64].

Acknowledgements

This work was supported by the U.S. Department of Energy (DOE), Office of Science, Basic Energy Sciences, Materials Science and Engineering Division. The research was performed at the Ames Laboratory, which is operated for the U.S. DOE by Iowa State University under Contract No. DE-AC02-07CH11358.

References

- [1] M. A. Nielsen, I. Chuang, *Quantum computation and quantum information*, American Association of Physics Teachers, **2002**.
- [2] A. Aspuru-Guzik, A. D. Dutoi, P. J. Love, M. Head-Gordon, *Science* **2005**, *309*, 5741 1704.
- [3] Y. Cao, J. Romero, J. P. Olson, M. Degroote, P. D. Johnson, M. Kieferová, I. D. Kivlichan, T. Menke, B. Peropadre, N. P. Sawaya, et al., *Chem. Rev.* **2019**, *119*, 19 10856.
- [4] S. McArdle, S. Endo, A. Aspuru-Guzik, S. C. Benjamin, X. Yuan, *Rev. Mod. Phys.* **2020**, *92* 015003.
- [5] A. Peruzzo, J. McClean, P. Shadbolt, M.-H. Yung, X.-Q. Zhou, P. J. Love, A. Aspuru-Guzik, J. L. O’Brien, *Nat. Commun.* **2014**, *5* 4213.
- [6] J. R. McClean, J. Romero, R. Babbush, A. Aspuru-Guzik, *New J. Phys.* **2016**, *18*, 2 023023.
- [7] J. R. McClean, M. E. Kimchi-Schwartz, J. Carter, W. A. De Jong, *Phys. Rev. A* **2017**, *95*, 4 042308.
- [8] R. Santagati, J. Wang, A. A. Gentile, S. Paesani, N. Wiebe, J. R. McClean, S. Morley-Short, P. J. Shadbolt, D. Bonneau, J. W. Silverstone, et al., *Sci. Adv.* **2018**, *4*, 1 eaap9646.
- [9] O. Higgott, D. Wang, S. Brierley, *Quantum* **2019**, *3* 156.
- [10] M. J. Beach, R. G. Melko, T. Grover, T. H. Hsieh, *Phys. Rev. B* **2019**, *100*, 9 094434.
- [11] M. Motta, C. Sun, A. T. Tan, M. J. O’Rourke, E. Ye, A. J. Minnich, F. G. Brandão, G. K.-L. Chan, *Nat. Phys.* **2020**, *16*, 2 205.

- [12] X. Yuan, S. Endo, Q. Zhao, Y. Li, S. C. Benjamin, *Quantum* **2019**, *3* 191.
- [13] S. McArdle, T. Jones, S. Endo, Y. Li, S. C. Benjamin, X. Yuan, *npj Quantum Inf.* **2019**, *5*, 1 1.
- [14] N. Gomes, F. Zhang, N. F. Berthussen, C.-Z. Wang, K.-M. Ho, P. P. Orth, Y.-X. Yao, *J. Chem. Theory Comput.* **2020**, *16*, 10 6256.
- [15] K. Yeter-Aydeniz, R. C. Pooser, G. Siopsis, *npj Quantum Inf.* **2020**, *6*, 1 1.
- [16] H. Nishi, T. Kosugi, Y.-i. Matsushita, *arXiv:2005.12715* **2020**.
- [17] S.-N. Sun, M. Motta, R. N. Tazhigulov, A. T. Tan, G. K. Chan, A. J. Minnich, *arXiv:2009.03542* **2020**.
- [18] A. Kandala, A. Mezzacapo, K. Temme, M. Takita, M. Brink, J. M. Chow, J. M. Gambetta, *Nature* **2017**, *549*, 7671 242.
- [19] P. K. Barkoutsos, J. F. Gonthier, I. Sokolov, N. Moll, G. Salis, A. Fuhrer, M. Ganzhorn, D. J. Egger, M. Troyer, A. Mezzacapo, et al., *Phys. Rev. A* **2018**, *98*, 2 022322.
- [20] J. Lee, W. J. Huggins, M. Head-Gordon, K. B. Whaley, *J. Chem. Theory Comput.* **2018**, *15*, 1 311.
- [21] D. Wecker, M. B. Hastings, M. Troyer, *Phys. Rev. A* **2015**, *92*, 4 042303.
- [22] E. Farhi, J. Goldstone, S. Gutmann, *arXiv:1411.4028* **2014**.
- [23] H. R. Grimsley, S. E. Economou, E. Barnes, N. J. Mayhall, In *Nat. Commun.* [25], 1–9.
- [24] I. G. Ryabinkin, T.-C. Yen, S. N. Genin, A. F. Izmaylov, *J. Chem. Theory Comput.* **2018**, *14*, 12 6317.
- [25] H. R. Grimsley, S. E. Economou, E. Barnes, N. J. Mayhall, *Nat. Commun.* **2019**, *10*, 1 1.
- [26] H. L. Tang, E. Barnes, H. R. Grimsley, N. J. Mayhall, S. E. Economou, *arXiv:1911.10205* **2019**.
- [27] Y. S. Yordanov, V. Armaos, C. H. Barnes, D. R. Arvidsson-Shukur, *arXiv:2011.10540* **2020**.
- [28] A. G. Rattew, S. Hu, M. Pistoia, R. Chen, S. Wood, *arXiv* **2019**, arXiv–1910.
- [29] M. Ostaszewski, E. Grant, M. Benedetti, *arXiv preprint arXiv:1905.09692* **2019**.
- [30] Y.-X. Yao, N. Gomes, F. Zhang, T. Iadecola, C.-Z. Wang, K.-M. Ho, P. P. Orth, *arXiv:2011.00622* **2020**.
- [31] M. Berman, R. Kosloff, *Comput. Phys. Commun.* **1991**, *63*, 1–3 1.
- [32] P. Jordan, E. P. Wigner, In *The Collected Works of Eugene Paul Wigner*, 109–129. Springer, **1993**.
- [33] S. B. Bravyi, A. Y. Kitaev, *Ann. Phys.* **2002**, *298*, 1 210.
- [34] J. T. Seeley, M. J. Richard, P. J. Love, *J. Chem. Phys.* **2012**, *137*, 22 224109.
- [35] Y. Li, S. C. Benjamin, *Phys. Rev. X* **2017**, *7*, 2 021050.
- [36] J. Romero, R. Babbush, J. R. McClean, C. Hempel, P. J. Love, A. Aspuru-Guzik, *Quantum Sci. Technol.* **2018**, *4*, 1 014008.
- [37] G. Ortiz, J. E. Gubernatis, E. Knill, R. Laflamme, *Phys. Rev. A* **2001**, *64* 022319.
- [38] K. Mitarai, K. Fujii, *Phys. Rev. Research* **2019**, *1*, 1 013006.
- [39] A. Mari, T. R. Bromley, N. Killoran, *arXiv:2008.06517* **2020**.
- [40] J. Li, X. Yang, X. Peng, C.-P. Sun, *Phys. Rev. Lett.* **2017**, *118*, 15 150503.

- [41] K. Mitarai, M. Negoro, M. Kitagawa, K. Fujii, *Phys. Rev. A* **2018**, *98*, 3 032309.
- [42] M. Schuld, V. Bergholm, C. Gogolin, J. Izaac, N. Killoran, *Phys. Rev. A* **2019**, *99*, 3 032331.
- [43] J. W. Demmel, *Applied numerical linear algebra*, SIAM, **1997**.
- [44] A. M. Childs, N. Wiebe, *arXiv:1202.5822* **2012**.
- [45] Q. Sun, T. C. Berkelbach, N. S. Blunt, G. H. Booth, S. Guo, Z. Li, J. Liu, J. D. McClain, E. R. Sayfutyarova, S. Sharma, et al., *Wiley Interdiscip. Rev.: Comput. Mol. Sci.* **2018**, *8*, 1 e1340.
- [46] A. Tranter, S. Sofia, J. Seeley, M. Kaicher, J. McClean, R. Babbush, P. V. Coveney, F. Mintert, F. Wilhelm, P. J. Love, *Int. J. Quantum Chem.* **2015**, *115*, 19 1431.
- [47] S. Bravyi, J. M. Gambetta, A. Mezzacapo, K. Temme, *arXiv:1701.08213* **2017**.
- [48] J. R. McClean, S. Boixo, V. N. Smelyanskiy, R. Babbush, H. Neven, *Nat. Commun.* **2018**, *9*, 1 1.
- [49] E. Grant, L. Wossnig, M. Ostaszewski, M. Benedetti, *Quantum* **2019**, *3* 214.
- [50] T. L. Patti, K. Najafi, X. Gao, S. F. Yelin, *arXiv:2012.12658* **2020**.
- [51] B. Peng, K. Kowalski, *J. Chem. Theory Comput.* **2017**, *13*, 9 4179.
- [52] M. Motta, E. Ye, J. R. McClean, Z. Li, A. J. Minnich, R. Babbush, G. K. Chan, *arXiv:1808.02625* **2018**.
- [53] W. J. Huggins, J. McClean, N. Rubin, Z. Jiang, N. Wiebe, K. B. Whaley, R. Babbush, *arXiv:1907.13117* **2019**.
- [54] J. Liu, Z. Li, J. Yang, *arXiv:2012.07047* **2020**.
- [55] C. J. Cramer, *Essentials of computational chemistry: theories and models*, John Wiley & Sons, **2013**.
- [56] Y.-X. Yao, F. Zhang, C.-Z. Wang, K.-M. Ho, P. P. Orth, *arXiv:2003.04211* **2020**.
- [57] N. Lanatà, Y.-X. Yao, C.-Z. Wang, K.-M. Ho, G. Kotliar, *Phys. Rev. X* **2015**, *5*, 1 011008.
- [58] N. Lanatà, Y. Yao, X. Deng, V. Dobrosavljević, G. Kotliar, *Phys. Rev. Lett.* **2017**, *118* 126401.
- [59] G. Knizia, G. K.-L. Chan, *Physical review letters* **2012**, *109*, 18 186404.
- [60] G. Knizia, G. K.-L. Chan, *Journal of chemical theory and computation* **2013**, *9*, 3 1428.
- [61] Q. Sun, G. K.-L. Chan, *Acc. Chem. Res.* **2016**, *49*, 12 2705.
- [62] T.-H. Lee, T. Ayril, Y.-X. Yao, N. Lanata, G. Kotliar, *Phys. Rev. B* **2019**, *99*, 11 115129.
- [63] J. MacDonald, *Phys. Rev.* **1934**, *46*, 9 828.
- [64] L.-W. Wang, A. Zunger, *J. Chem. Phys.* **1994**, *100*, 3 2394.